

# Fractional quantum Hall states of few bosonic atoms in geometric gauge fields

B. Juliá-Díaz<sup>1,2</sup>, T. Graß<sup>2</sup>, N. Barberán<sup>1</sup>, and M. Lewenstein<sup>2,3</sup>

<sup>1</sup> Departament d'Estructura i Constituents de la Matèria, Facultat de Física, Universitat de Barcelona, E-08028, Barcelona, Spain

<sup>2</sup> ICFO-Institut de Ciències Fotòniques, Parc Mediterrani de la Tecnologia, 08860 Barcelona, Spain

<sup>3</sup>ICREA-Institució Catalana de Recerca i Estudis Avançats, 08010 Barcelona, Spain

## Abstract.

We employ the exact diagonalization method to analyze the possibility of generating strongly correlated states in two-dimensional clouds of ultracold bosonic atoms which are subjected to a geometric gauge field created by coupling two internal atomic states to a laser beam. Tuning the gauge field strength, the system undergoes stepwise transitions between different ground states, which we describe by analytical trial wave functions, amongst them the Pfaffian, the Laughlin, and a Laughlin quasiparticle many-body state. The adiabatic following of the center of mass movement by the lowest energy dressed internal state, is lost by the mixing of the second internal state. This mixture can be controlled by the intensity of the laser field. The non-adiabaticity is inherent to the considered setup, and is shown to play the role of circular asymmetry. We study its influence on the properties of the ground state of the system. Its main effect is to reduce the overlap of the numerical solutions with the analytical trial expressions by occupying states with higher angular momentum. Thus, we propose generalized wave functions arising from the Laughlin and Pfaffian wave function by including components, where extra Jastrow factors appear, while preserving important features of these states. We analyze quasihole excitations over the Laughlin and generalized Laughlin states, and show that they possess effective fractional charge and obey anyonic statistics. Finally, we study the energy gap over the Laughlin state as the number of particles is increased keeping the chemical potential fixed. The gap is found to decrease as the number of particles is increased, indicating that the observability of the Laughlin state is restricted to a small number of particles.

## 1. Introduction

A spectacular progress on the manipulation and control of cold atomic clouds has been achieved since the first experimental realization of a Bose-Einstein condensed system by Anderson *et al.* [1] and Davis *et al.* [2] nearly simultaneously in 1995. On the one hand, these systems provide us with a toolbox for studying the principles of quantum mechanics, as has for instance been done in experiments involving the interference of two condensates leading to the manifestation of coherence [3]. On the other hand, cold atoms have been used in order to simulate interesting phenomena appearing in condensed-matter physics [4], like the Mott-insulator to superfluid transition [5].

A severe restriction, however, stems from the atom's electro-neutrality, which hinders a direct implementation of phenomena involving electromagnetic forces. An important example of the latter is the physics of the integer and fractional quantum Hall effect, occurring in two-dimensional interacting systems under the presence of a strong perpendicular magnetic field. The ground states of fractional quantum Hall (FQHE) systems are highly correlated states, like the Pfaffian state proposed by Moore and Read [6], or the celebrated Laughlin state [7], whose bosonic analogs are found to be the exact eigenstates of a Hamiltonian with a three-body (3B), or two-body (2B) [8, 9] contact interaction, respectively. In addition, the quasihole excitations over the Laughlin state have fractional effective charge and fractional statistics [10]. Excitations of the Pfaffian state may even obey non-Abelian braiding statistics [11, 12], which makes them interesting from both fundamental and technological points of view [13].

Several proposals of experimental routes to obtain these types of states have appeared in the literature, ranging from the use of rotating traps to simulate magnetic fields acting on charges to the use of laser-beam configurations acting on atoms with several internal states [14, 15, 16, 17, 18, 19, 20, 21]. In this article we analyze the appropriate conditions to realize some strongly correlated states within a simple configuration of a single laser beam shining on a cloud of cold atoms with two internal states. If the internal dynamics of the atoms, governed by the Rabi frequency of the atom-laser coupling, is fast enough with respect to the slow variation of center of mass position, then the atoms evolve adiabatically. They remain in one definite space-dependent superposition of the internal bare states, and the accumulation of Berry phase [22] during its movement mimics an effective magnetic field [23, 24]. An important goal is to go further and analyze the effect of a slight amount of non-adiabaticity, which we treat in a perturbative way.

Through the controlled variation of external parameters, different strongly correlated states appear in the spectrum, i.e. a Laughlin-like state, a Pfaffian-like state and the quasiparticle-like state obtained from the Laughlin. Our main aim is to map the regions in parameter space where the exact, numerically obtained, ground state (GS) has a large overlap with explicit analytical expressions provided for these relevant strongly correlated states. To remain close to possible experimental implementations, we study the effect of small perturbations that create non-adiabaticities which are unavoidable

for finite values of the laser intensity. The small perturbation produces a deformation of the atomic cloud preserving most of the notable properties of the original states, e.g. entropy, internal energy, or anyonic character of excitations. These slightly asymmetric ground states are well represented by generalized analytic wave functions.

Focusing additional laser beams on the atomic cloud, it is possible to pierce holes into the system. As long as the asymmetric perturbation is small, the resulting states can be well described by an analytical quasihole wave function, which can be obtained from the Laughlin or the generalized Laughlin wave function. In both cases, the effective charge and statistical phase of the quasihole excitations are found to attain fractional values, demonstrating the possibility of observing anyons within the proposed setup.

In this work we concentrate on the physics of few-body systems, independently of their attainability in the thermodynamic limit, which is beyond the scope of the present article. This approach is meaningful as there are nowadays a number of groups able of dealing with small bosonic clouds using several techniques [25, 26]. In particular, Ref. [26] has presented experimental evidence for the production of quantum states of fractional quantum Hall type for small atom systems ( $N < 10$ ). These experimental developments have triggered a number of theoretical proposals focusing on the production of strongly correlated quantum states in small atomic clouds [16, 19, 20]. We analyze the dependence on the number of particles of some of our main results. First, we show that observing the anyonic character of quasihole excitations becomes possible when  $N \gtrsim 5$ . Second, we show that at fixed chemical potential the bulk gap of the Laughlin state is decreased as  $N$  is increased, indicating that few-body systems provide the best scenario for producing the bosonic Laughlin state.

The paper is organized as follows. In Section 2 we present the system and derive an effective Hamiltonian to describe it. In Section 3 we provide the analytical expressions of the relevant fractional quantum Hall states and their generalizations. Our results are presented in Section 4 and Section 5 in the adiabatic/symmetric and non-adiabatic/asymmetric cases, respectively. In Section 6 we study the fractional charge and anyonic statistics of quasiholes, produced by means of additional lasers. In Section 7 we analyze the behavior of the energy gap above the Laughlin state as  $N$  increases, and its evolution as a function of the system's parameters. Finally, in Section 8, we present our conclusions.

## 2. Description of the system

We consider a setup to produce artificial gauge fields in a small cloud of ultracold atoms closely following the configuration described in Ref. [21]. The system is confined by harmonic traps. The confinement in the  $z$  direction is assumed to be strong enough to achieve effectively a two dimensional system. The cloud is illuminated by a single laser beam with wave number  $k$  and frequency  $\omega_L$ , which propagates in the  $y$ -direction and is close to the resonance with a transition between two internal atomic states,  $\omega_L = \omega_A$ . The interaction between the electric field of the laser and the induced electric dipole is

modeled by the atom-laser Hamiltonian, which in the rotating-wave approximation and in the rotating frame is given by [27, 28],

$$H_{\text{AL}} = E_g |g\rangle \langle g| + (E_e - \hbar\omega_L) |e\rangle \langle e| + \frac{\hbar\Omega_0}{2} e^{iky} |e\rangle \langle g| + \frac{\hbar\Omega_0}{2} e^{-iky} |g\rangle \langle e| \quad (1)$$

where  $E_g$  and  $E_e$  are the energies of the bare atomic ground and excited state and  $\Omega_0$  is the Rabi frequency, which is proportional to the laser intensity. No spontaneous emission of photons from the excited state is considered. This assumption is justified as long as the lifetime of the excited state is longer than the typical duration of an experiment. Lifetimes of several seconds, as found for Ytterbium or some Alkaline earth metals, should be sufficient.

In order to obtain a non-trivial gauge potential from the coupling in Eq. (1), we still have to make it dependent on  $x$ . This can be achieved via a real magnetic field, which by Zeeman effect makes the internal energy levels vary linearly with  $x$ . Introducing a parameter  $w$ , setting the length scale of this shift, we have,

$$E_g = -\frac{\hbar\Omega_0}{2} \frac{x}{w}, \quad E_e = \hbar\omega_A + \frac{\hbar\Omega_0}{2} \frac{x}{w}. \quad (2)$$

Then, the single particle Hamiltonian is given by

$$H_{\text{sp}} = \frac{p^2}{2M} + V(\vec{r}) + \frac{\hbar\Omega}{2} \begin{pmatrix} \cos \theta & e^{i\phi} \sin \theta \\ e^{-i\phi} \sin \theta & -\cos \theta \end{pmatrix}, \quad (3)$$

where the third term is the atom-laser Hamiltonian represented in the  $\{|e\rangle, |g\rangle\}$  basis. Here,  $M$  is the atomic mass,  $\Omega = \Omega_0 \sqrt{1 + x^2/w^2}$ ,  $\sin \theta = w/\sqrt{w^2 + x^2}$ ,  $\cos \theta = x/\sqrt{w^2 + x^2}$ , and  $\phi = ky$ .  $V(\vec{r})$  is the trap potential that will be fixed below.

Up to this point, the Hamiltonian is given by physically measurable parameters. In the next step, we choose particular expressions for the single particle states that diagonalize the atom-laser Hamiltonian. This corresponds in fact to the selection of a specific gauge for the vector and scalar potentials that will drive the center of mass dynamics, as will be shown below. We consider the eigenfunctions of  $H_{\text{AL}}$  given by,

$$|\Psi_1\rangle = e^{-iG} \begin{pmatrix} C e^{i\phi/2} \\ S e^{-i\phi/2} \end{pmatrix}, \quad |\Psi_2\rangle = e^{iG} \begin{pmatrix} -S e^{i\phi/2} \\ C e^{-i\phi/2} \end{pmatrix}, \quad (4)$$

in the  $\{|e\rangle, |g\rangle\}$  basis, where  $C = \cos \theta/2$ ,  $S = \sin \theta/2$ , and  $G = \frac{kxy}{4w}$ . The atomic state can be then expressed as,

$$\chi(\vec{r}) = a_1(\vec{r}) \otimes |\Psi_1\rangle + a_2(\vec{r}) \otimes |\Psi_2\rangle \quad (5)$$

where  $a_i$  captures the external dynamics and  $|\Psi_i\rangle$  provides internal degree of freedom. The single-particle Hamiltonian is then expressed in the  $\{|\Psi_1\rangle, |\Psi_2\rangle\}$  basis as

$$H_{\text{sp}} = \begin{pmatrix} H_{11} & H_{12} \\ H_{21} & H_{22} \end{pmatrix}, \quad (6)$$

acting on the spinor  $[a_1(\vec{r}), a_2(\vec{r})]$ . Defining a vector potential  $\vec{A}$ ,

$$\vec{A}(\vec{r}) = \hbar k \left[ \frac{y}{4w}, \frac{x}{4w} - \frac{x}{2\sqrt{x^2 + w^2}} \right] \quad (7)$$

and a scalar potential  $U$ ,

$$U(\vec{r}) = \frac{\hbar^2 w^2}{8M(x^2 + w^2)} \left( k^2 + \frac{1}{x^2 + w^2} \right), \quad (8)$$

we obtain,

$$H_{11} = \frac{[\vec{p} - \vec{A}(\vec{r})]^2}{2M} + U(\vec{r}) + V(\vec{r}) + \frac{\hbar\Omega(\vec{r})}{2}, \quad (9)$$

and

$$H_{22} = \frac{[\vec{p} + \vec{A}(\vec{r})]^2}{2M} + U(\vec{r}) + V(\vec{r}) - \frac{\hbar\Omega(\vec{r})}{2}, \quad (10)$$

which are the Hamiltonians driving the external dynamics of atoms being in the internal state  $|\Psi_1\rangle$  and  $|\Psi_2\rangle$ , respectively. By expanding the  $H_{ij}$  terms up to second order in  $x$  and  $y$ , which is justified by choosing  $w$  to be larger than the extension of the cloud, we find that the energy distance between these two manifolds is given by  $\hbar\Omega_0$ . For convenience, we make the Hamiltonian element for the low energy manifold,  $H_{22}$ , independent of  $\Omega_0$  by adding the constant term  $\frac{\hbar\Omega_0}{2}$  to the diagonal of  $\hat{H}_{\text{sp}}$ . Further we note that with the explicit selection of Eq. (4) and for  $x, y \ll w$ ,  $\vec{A}$  is in the symmetric gauge:  $\vec{A} \approx \frac{\hbar k}{4w}(y, -x)$ . This allows for making  $H_{22}$  fully symmetric by a proper choice of the trapping frequency. Eq. (10) then takes the form

$$H_{22} = \frac{p^2}{2M} + \frac{\vec{p} \cdot \vec{A}}{M} + \frac{M}{2}\omega_{\perp}(x^2 + y^2), \quad (11)$$

and we can take the advantage from the knowledge of its single particle eigenfunctions, namely the Fock-Darwin states [32]. This final expression is formally equal to the Hamiltonian driving a system of charges trapped by a harmonic potential of frequency  $\omega_{\perp}$ , under a constant magnetic field along the  $z$ -direction, or equivalently, a system of neutral atoms trapped by a rotating harmonic potential of frequency  $\omega_{\perp}$ , expressed in the rotating frame of reference [33, 34].

While the equivalence to the rotating case holds for  $H_{22}$ , we stress that it does not for the system's behavior in the upper manifold described by  $H_{11}$ . However, due to the off-diagonal terms in  $\hat{H}_{\text{sp}}$ , both manifolds are coupled. Typical expected values of  $H_{12}$  and  $H_{21}$  are of the order of the recoil energy  $E_R = \frac{\hbar^2 k^2}{2M}$  which gives the scale for the kinetic energy of the atomic center-of-mass motion when it absorbs or emits a single photon. If we consider  $\hbar\Omega_0 \gg E_R$ , this coupling is small, and we can restrict ourselves to the low energy manifold. Namely, we are in the situation where the internal dynamics is much faster than the center of mass motion and can follow the external variations in a quasiadiabatic way [29].

To go beyond the adiabatic approximation, we consider the influence of the high-energy manifold as a small perturbation. Using the procedure appropriate to systems that show two significantly different energy scales as explained in Ref. [27], and detailed

in Appendix A, we calculate an effective Hamiltonian up to second order in the perturbation, which reads

$$H_{22}^{\text{eff}} = H_{22} - \frac{H_{21}H_{12}}{\hbar\Omega_0}, \quad (12)$$

where the explicit expression for the perturbative term  $H_{21}H_{12}/\Omega_0$  is given in Appendix A. Though mathematically more involved and physically richer, this term is reminiscent of the anisotropic potential that is applied to set an atomic cloud in rotation. Usually, the expression used to model the stirring laser is given by  $\alpha M\omega_\perp(x^2 - y^2)$  [30, 31], where  $\alpha$  measures the strength of the deformation. Similarly the term  $H_{21}H_{12}/\hbar\Omega_0$  can only produce changes of  $L$  of  $\Delta L = 0, \pm 2, \pm 4$  (see Appendix A). In what follows we will identify 'deformation' with 'coupling' indicating that a large connection with  $H_{11}$  implies deformation since  $H_{11}$  is not cylindrically symmetric.

The many-body Hamiltonian which we finally will deal with is given by adding a contact interaction term to the effective Hamiltonian from Eq. (12):

$$H = \sum_{i=1}^N H_{22}^{\text{eff}}(i) + \frac{\hbar^2 g}{M} \sum_{i < j} \delta(\vec{r}_i - \vec{r}_j) \quad (13)$$

where  $g$  is a dimensionless parameter fixing the contact interaction strength. From now on we will consider  $gN = 6$  in the numerical calculations. The Hamiltonian  $H$  acts only on the low energy manifold, which effectively is perturbed by the second manifold. The important two parameters in  $H$  are the dimensionless ratio  $\eta \equiv \frac{\hbar k}{4Mw\omega_\perp}$  and the degree of the perturbation given by  $\Omega_0$ . The expression  $\eta\omega_\perp$  plays the role of the rotating frequency, and also the effective magnetic field strength  $B_0$  is proportional to  $\eta$ :

$$B_0 \equiv \frac{\hbar k}{2w} = 2M\omega_\perp\eta. \quad (14)$$

The largest possible value of  $\eta$  is given by 1 in order to keep the system confined. We consider that the artificial magnetic field is strong enough to work exclusively in the lowest Landau level regime. To this end, our parameters must fulfill the following conditions: the energy difference between Landau levels is larger than both, the kinetic energy of a single particle within a Landau level and the interaction energy per particle. Note that the strength of the atom-laser coupling, characterized by  $\Omega_0$ , is different from the strength of the magnetic field, characterized by  $\eta$ . Because the magnetic field has a geometric origin,  $\eta$  is independent of the atom-laser coupling, as long as the adiabatic approximation is justified.

### 3. Analytical many-body states

In this section we give an overview of the analytical wave functions discussed in the literature which will turn out to be relevant for describing our system.

### 3.1. Laughlin state

The well-known Laughlin state has the analytical form [7, 35, 36],

$$\Psi_{\mathcal{L}}(z_1, \dots, z_N) = \mathcal{N}_{\mathcal{L}} \prod_{i < j} (z_i - z_j)^{1/\nu} e^{-\sum |z_i|^2 / 2\lambda_{\perp}^2}, \quad (15)$$

where  $\mathcal{N}_{\mathcal{L}}$  is a normalization constant,  $z = x + iy$  and  $\lambda_{\perp} = \sqrt{\hbar/M\omega_{\perp}}$ . The inverse of the exponent,  $\nu$ , fixes both the density of the system and the symmetry of the wave function. For bosons,  $1/\nu$  must be even. The Laughlin regime discussed here will be at half filling, so for the rest of this paper we set  $\nu = \frac{1}{2}$ .

The analysis of the squared overlap  $|\langle \Psi_{\mathcal{L}} | \text{GS} \rangle|^2$  of the Laughlin state with the exact ground state as a function of the artificial magnetic field strength  $\eta$  and the atom-laser coupling  $\Omega_0$  shows that the overlap gets reduced as  $\hbar\Omega_0/E_R$  decreases, even for large values of  $\eta$ . Larger overlap with the ground state can be obtained by adding an admixture of the Laughlin state with additional Jastrow factors that allow for an increase of total angular momentum, which in the Laughlin state is given by the integer  $L = \frac{N(N-1)}{2\nu}$ . Based on these observations, in Ref. [21] an analytical ansatz for the ground state in the Laughlin-like region ‡ was proposed,

$$\Psi_{\mathcal{GL}} = \alpha \Psi_{\mathcal{L}} + \beta \Psi_{\mathcal{L}1} + \gamma \Psi_{\mathcal{L}2}, \quad (16)$$

from here on referred to as the generalized Laughlin (GL) state, with  $\Psi_{\mathcal{L}1} = \mathcal{N}_1 \Psi_{\mathcal{L}} \cdot \sum_{i=1}^N z_i^2$ ,  $\Psi_{\mathcal{L}2} = \mathcal{N}_2 (\tilde{\Psi}_{\mathcal{L}2} - \langle \Psi_{\mathcal{L}1} | \tilde{\Psi}_{\mathcal{L}2} \rangle \Psi_{\mathcal{L}1})$ , and  $\tilde{\Psi}_{\mathcal{L}2} = \tilde{\mathcal{N}}_2 \Psi_{\mathcal{L}} \cdot \sum_{i < j}^N z_i z_j$ , such that we ensure  $\langle \Psi_{\mathcal{L}} | \Psi_{\mathcal{L}i} \rangle = 0$  and  $\langle \Psi_{\mathcal{L}i} | \Psi_{\mathcal{L}j} \rangle = \delta_{ij}$ . This ansatz involves components of angular momentum  $L = N(N-1)$  and  $L = N(N-1) + 2$ , and yields zero contact interaction energy. The values of  $\alpha$ ,  $\beta$  and  $\gamma$  are computed as  $\alpha = \langle \Psi_{\mathcal{L}} | \text{GS} \rangle / \sqrt{\mathcal{N}}$ ,  $\beta = \langle \Psi_{\mathcal{L}1} | \text{GS} \rangle / \sqrt{\mathcal{N}}$ , and  $\gamma = \langle \Psi_{\mathcal{L}2} | \text{GS} \rangle / \sqrt{\mathcal{N}}$ , with  $\mathcal{N} = |\langle \Psi_{\mathcal{L}} | \text{GS} \rangle|^2 + |\langle \Psi_{\mathcal{L}1} | \text{GS} \rangle|^2 + |\langle \Psi_{\mathcal{L}2} | \text{GS} \rangle|^2$ .

### 3.2. Pfaffian (Moore-Read) state

While the Laughlin and the generalized Laughlin state turn out to be good trial states for strong magnetic fields  $\eta \lesssim 1$ , for smaller field strengths the Laughlin quasiparticle (LQP) state and the Pfaffian (Pf) state become relevant. The Pfaffian state has  $L = N(N-2)/2$  for even  $N$ , and  $L = (N-1)^2/2$  for odd  $N$  and its analytical expression reads,

$$\Psi_{\mathcal{P}} = \mathcal{N}_{\text{pf}} \text{Pf}([z]) \prod_{i < j} (z_i - z_j) \quad (17)$$

with  $\mathcal{N}_{\text{pf}}$  a normalization constant, and

$$\text{Pf}([z]) = \mathcal{A} \left[ \frac{1}{(z_1 - z_2)} \frac{1}{(z_3 - z_4)} \cdots \frac{1}{(z_{N-1} - z_N)} \right], \quad (18)$$

where  $\mathcal{A}$  is an antisymmetrizer of the product. As explained in Ref. [8, 9], the Pfaffian state can also be computed as,

$$\Psi_{\mathcal{P}} = \mathcal{S} \prod_{i < j \in \sigma_1} (z_i - z_j)^2 \prod_{k < l \in \sigma_2} (z_k - z_l)^2 \quad (19)$$

‡ Defined as the parameter domain where  $\langle L \rangle \geq N(N-1)$ .



where  $\sigma_1$  and  $\sigma_2$  are two subsets containing  $N/2$  particles each if  $N$  is even, and  $(N+1)/2$  and  $(N-1)/2$  if  $N$  is odd.  $\mathcal{S}$  symmetrizes the expression. The Pfaffian state has been shown to be the lowest energy eigenstate of a Hamiltonian which contains only three-body contact interactions [6, 20],

$$H_{\text{int}} = \sum_{i < j < k} \delta(z_i - z_j) \delta(z_j - z_k), \quad (20)$$

and, similarly to the Laughlin with the two-body interaction, it has zero three-body interaction energy. Remarkably, however, as shown in Refs. [8, 16] for a two-body interaction Hamiltonian and for some values of  $\eta$  there is a sizeable overlap between the ground state of the system and this state.

As we did before for the Laughlin state in Eq. (16), we can define a generalized Pfaffian (GPf) state as

$$\Psi_{\mathcal{GP}} = \alpha \Psi_{\mathcal{P}} + \beta \Psi_{\mathcal{P}1} + \gamma \Psi_{\mathcal{P}2}, \quad (21)$$

with  $\Psi_{\mathcal{P}1} = \mathcal{N}_{\mathcal{P}1} \Psi_{\mathcal{P}} \cdot \sum_{i=1}^N z_i^2$ ,  $\Psi_{\mathcal{P}2} = \mathcal{N}_{\mathcal{P}2} (\tilde{\Psi}_{\mathcal{P}2} - \langle \Psi_{\mathcal{P}1} | \tilde{\Psi}_{\mathcal{P}2} \rangle \Psi_{\mathcal{P}1})$ , and  $\tilde{\Psi}_{\mathcal{P}2} = \tilde{\mathcal{N}}_{\mathcal{P}2} \Psi_{\mathcal{P}} \cdot \sum_{i < j}^N z_i z_j$ . Again, the parameters  $\alpha$ ,  $\beta$ , and  $\gamma$  are fixed to maximize the overlap of the numerical ground state with  $\Psi_{\mathcal{GP}}$ .

### 3.3. Laughlin-quasiparticle state

The Laughlin-quasiparticle state arises from the Laughlin state by increasing the density at the origin, decreasing its angular momentum,  $L_{\text{qp}} = N(N-1) - N$ . The latter formula holds if the quasiparticle is at the origin. Otherwise, it also carries angular momentum and the total expected value of the angular momentum of the system is no longer an integer. The wave function is written as,

$$\Psi_{\mathcal{Lqp}} = \mathcal{N}_{\text{qp}}(\xi, \xi^*) (\partial_{z_1} - \xi) \cdots (\partial_{z_N} - \xi) \Psi_{\mathcal{L}}, \quad (22)$$

with  $\mathcal{N}_{\text{qp}}(\xi, \xi^*)$  a normalization constant that depends on the position  $\xi$  and  $\xi^*$  of the excitation. Also for the Laughlin-quasiparticle state we define a generalized version (GLQP), built up from the same Jastrow factors used in Eq. (16), i.e.

$$\Psi_{\mathcal{GLqp}} = \alpha \Psi_{\mathcal{Lqp}} + \beta \Psi_{\mathcal{Lqp}1} + \gamma \Psi_{\mathcal{Lqp}2}, \quad (23)$$

with  $\Psi_{\mathcal{Lqp}1} = \mathcal{N}_{\mathcal{Lqp}1} \Psi_{\mathcal{Lqp}} \cdot \sum_{i=1}^N z_i^2$ ,  $\Psi_{\mathcal{Lqp}2} = \mathcal{N}_{\mathcal{Lqp}2} (\tilde{\Psi}_{\mathcal{Lqp}2} - \langle \Psi_{\mathcal{Lqp}1} | \tilde{\Psi}_{\mathcal{Lqp}2} \rangle \Psi_{\mathcal{Lqp}1})$ , and  $\tilde{\Psi}_{\mathcal{Lqp}2} = \tilde{\mathcal{N}}_{\mathcal{Lqp}2} \Psi_{\mathcal{Lqp}} \cdot \sum_{i < j}^N z_i z_j$ .

### 3.4. Laughlin-quasihole state

Alternatively to increasing the homogeneous density of the Laughlin state locally, one might also decrease it by piercing a hole in the atomic cloud. Formally this is achieved by introducing an additional zero into the wave function, multiplying it with  $\prod_i (\xi - z_i)$ . The resulting quasihole state pierced at  $\xi$  reads:

$$\Psi_{\mathcal{Lqh}} = \mathcal{N}_{\mathcal{Lqh}}(\xi, \xi^*) \prod_{i=1}^N (\xi - z_i) \Psi_{\mathcal{L}}, \quad (24)$$



where  $\mathcal{N}_{\mathcal{L}\text{qh}}(\xi, \xi^*)$  is a normalization constant, which explicitly depends on the position of the quasihole. To test the anyonic nature of the quasiholes, we need to do the same operation twice, such that the presence of two quasiholes is described by,

$$\Psi_{\mathcal{L}2\text{qh}} = \mathcal{N}_{\mathcal{L}2\text{qh}}(\xi_1, \xi_1^*, \xi_2, \xi_2^*) \prod_{i=1}^N (\xi_1 - z_i)(\xi_2 - z_i) \Psi_{\mathcal{L}}. \quad (25)$$

The state with one quasihole has a fixed total angular momentum, which is  $N$  quanta above the ground state, if the quasihole is at the origin,  $\xi = 0$ . For off-centered quasihole positions, the average angular momentum is slightly reduced and non-integer. The state with two quasiholes has an angular momentum close to  $2N$  quanta above the ground state.

We may also apply the same operation to the generalized Laughlin state and define,

$$\Psi_{\mathcal{G}\mathcal{L}\text{qh}} = \mathcal{N}_{\mathcal{G}\mathcal{L}\text{qh}}(\xi, \xi^*) \prod_{i=1}^N (\xi - z_i) [\alpha \Psi_{\mathcal{L}} + \beta \Psi_{\mathcal{L}1} + \gamma \Psi_{\mathcal{L}2}] \quad (26)$$

for the state with one quasihole, and

$$\begin{aligned} \Psi_{\mathcal{G}\mathcal{L}2\text{qh}} &= \mathcal{N}_{\mathcal{G}\mathcal{L}2\text{qh}}(\xi_1, \xi_1^*, \xi_2, \xi_2^*) \\ &\times \prod_{i=1}^N (\xi_1 - z_i)(\xi_2 - z_i) [\alpha \Psi_{\mathcal{L}} + \beta \Psi_{\mathcal{L}1} + \gamma \Psi_{\mathcal{L}2}] \end{aligned} \quad (27)$$

for the state with two quasiholes. As explained in Sec. 5, we always find  $\alpha, \beta \gg \gamma$ , thus in practice we will consider always  $\gamma \equiv 0$ .

#### 4. Results for the adiabatic/symmetric case, $H_{22}^{\text{eff}} = H_{22}$

In the symmetric case, in which the perturbation  $H_{21}H_{12}/(\hbar\Omega_0)$  is not included, and for  $N = 4$ , four distinct regions are detected depending on the value of  $\eta$  as previously obtained in Ref. [8, 16]: Condensed, Pfaffian, Laughlin-quasiparticle and Laughlin regime. We analyze them in the following Figs. 1 and 2.

The first region corresponds to a fully condensed system with zero angular momentum and vanishing one-body entanglement entropy §, see Fig. 1. The ground state can be well described by a wave function given by  $\Psi_C = \mathcal{N}_C e^{-\sum_i z_i^2/2\lambda_{\perp}}$  being  $\mathcal{N}_C$  a normalization constant.

Figs. 1 (middle panel) and 2 show that the first excitation is of quadrupolar character up to  $\eta = 0.7$ . Lower values of  $\eta$  lie beyond our lowest Landau level approximation, where a larger Hilbert space including more Landau levels has to be considered.

At the critical value  $\eta_1 = 1 - gN/(8\pi) \sim 0.76$ , ( $gN = 6$ ), a degeneracy between states with  $L = 0, 2, 3$ , and 4 occurs, see Fig. 2. At this  $\eta_1$  a state with broken

§ The entropy is defined here from the one-body density matrix, as  $S = -\sum n_i \ln(n_i)$ , where  $n_i$  are the eigenvalues of the one-body density matrix. For a more detailed discussion of the entropy we refer for instance to [21].

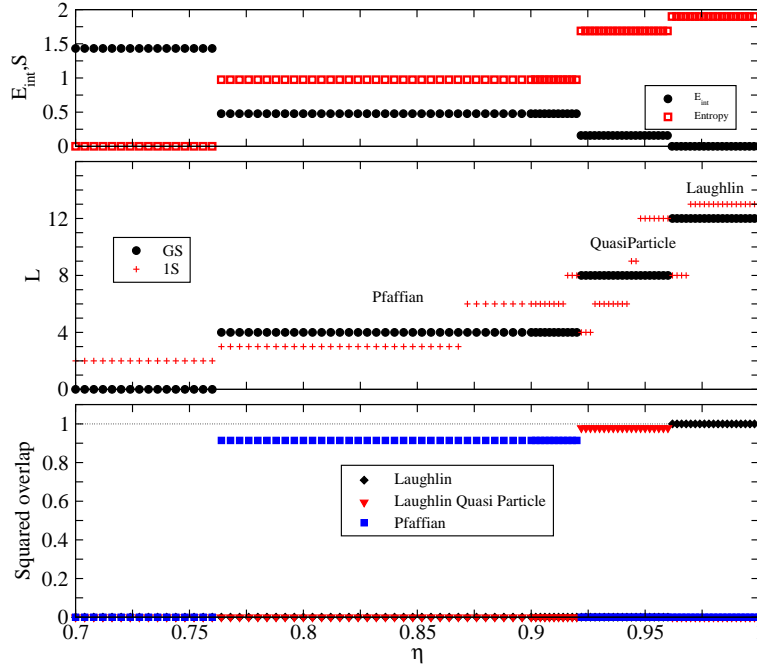


**Figure 1.** (Color online) (upper panel) Interaction energy in units of  $\hbar\omega_{\perp}$  (black circles) and one-body entanglement entropy (red squares) of the ground state as a function of  $\eta$ . (middle panel) Angular momentum in units of  $\hbar$  of the ground state and of the first excited state as a function of  $\eta$ . (lower panel) Squared overlap between the ground state of the system and the exact Laughlin, Pfaffian and Laughlin-quasiparticle states. The plots corresponds to the case  $H_{22}^{\text{eff}} = H_{22}$ .

symmetry, combination of several  $L$ -eigenstates, is precursor of the nucleation of the first vortex state. For increasing  $\eta$  the ground state recovers the cylindrical symmetry and the angular momentum is  $L = 4$ . All this phenomenology can be inferred from the Yrast line displayed in Fig. 3. The Yrast line is constructed by plotting the interaction energy contribution of the lowest energy state for each  $L$ . From this line, the addition of the kinetic energy, which reads (up to a term independent of  $L$  and  $\eta$ )  $E_{\text{kin}} = (1 - \eta)L\hbar\omega_{\perp}$ , produces the total energy with its minimum at the angular momentum of the ground state,  $L_{GS}$ , as exemplified for  $\eta = 0.85$  and  $0.94$  in Fig. 3. This is a general behavior for any  $N$ .

As  $\eta$  is increased above  $\eta_1$ , the ground state with  $L = 4$  becomes correlated as marked by the sizeable entanglement entropy (see Fig. 1), meaning that it is not fully condensed. Remarkably, its squared overlap with the Pfaffian state is much larger (about 0.9, see Fig. 4) as already noticed in Ref. [8, 16], than its squared overlap with the one-vortex-state (about 0.47), given by  $\Psi_{\text{1vx}} = \mathcal{N}_{\text{1vx}} \prod_{i=1}^N z_i e^{-\sum_i z_i^2 / 2\lambda_{\perp}}$  (being  $\mathcal{N}_{\text{1vx}}$  a normalization constant). If the ground state in this region is modeled by the eigenstate of the one-body density matrix with the highest occupation which plays the role of the order parameter in a mean field approach, it shows a well defined vortex at the center of the density distribution. The phase of the order parameter changes by  $2\pi$ , indicating

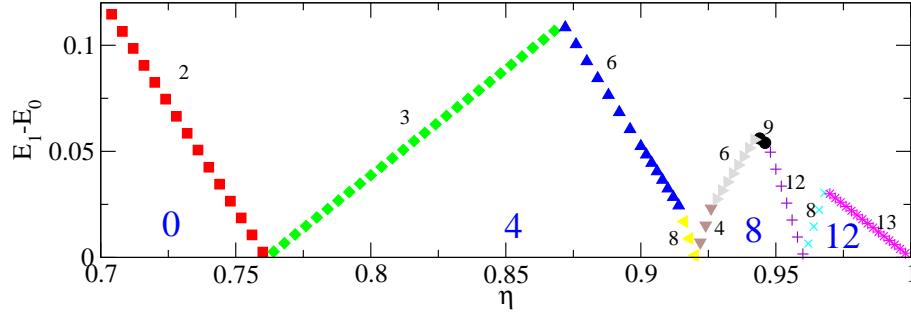


**Figure 2.** (Color online) Energy difference, in units of  $\hbar\omega_{\perp}$ , between the ground state and its first excitation as a function of  $\eta$ . The large blue numbers correspond to the value of  $L$  for the ground state. The small numbers quote the value of  $L$  of the first excited state.  $H_{22}^{\text{eff}} = H_{22}$ .

the existence of a vortex. However, this function is a poor representation of the ground state since the non-condensed fraction is significant. This region has three different kind of excitations,  $L = 3, 6$  and  $8$  as can be seen in Fig. 2. The latter has a large overlap with the Laughlin-quasiparticle state as can be seen in Fig. 4.

For  $0.92 \leq \eta \leq 0.96$ , the ground state has  $L = 8$ , a higher entanglement entropy, and a smaller interaction energy. The ground state has a large overlap with the Laughlin-quasiparticle state, as shown in Figs. 1 and 4. This quasiparticle region has four different excitations,  $L = 4, 6, 9$  and  $12$ . The  $L = 9$  corresponds to a center of mass excitation of the system as dictated by Kohn's theorem [32, 37].

Finally, for  $\eta \geq \eta_2 \simeq 0.96$ , the ground state wave function is the Laughlin wave function, with zero interaction energy. Its excitations are the Laughlin-quasiparticle  $L = 8$  and an a center of mass excitation, Kohn mode, with  $L = 13$ , whose analytical form is,  $\Psi = \mathcal{N}(z_1 + z_2 + z_3 + z_4)\Psi_{\mathcal{L}}$ .

## 5. Effects of the non-adiabaticity/asymmetry, $H_{22}^{\text{eff}} = H_{22} - H_{21}H_{12}/(\hbar\Omega_0)$ .

As discussed in Section 2 and Appendix A, the considered setup can be mapped onto a symmetric Hamiltonian,  $H_{22}$ , equivalent to the one of rotating atomic clouds in symmetric traps, plus a term,  $H_{21}H_{12}/(\hbar\Omega_0)$  whose importance can be controlled by tuning the laser coupling,  $\Omega_0$ . As discussed in Ref. [21], the first effect of the perturbation in the Laughlin-like region is to increase the angular momentum of the ground state by populating the states  $\Psi_{\mathcal{L}1}$ , defined in Eq. (16). One can consider fairly small coupling  $\hbar\Omega_0/E_R \sim 40$  and still get Laughlin-like ground states of the form of Eq. (16), which retain most of the known properties of Laughlin states, namely, a large entanglement entropy and vanishing interaction energy [21]. Now we extend the previous study to the effect of the perturbation on the Pfaffian and Laughlin-quasiparticle regions.

In Fig. 5 we show the squared overlap between the ground state and the three original correlated states (left panel) and their generalized versions (right panel) identified as the generalized Pfaffian, generalized Laughlin-quasiparticle (GLQP) and

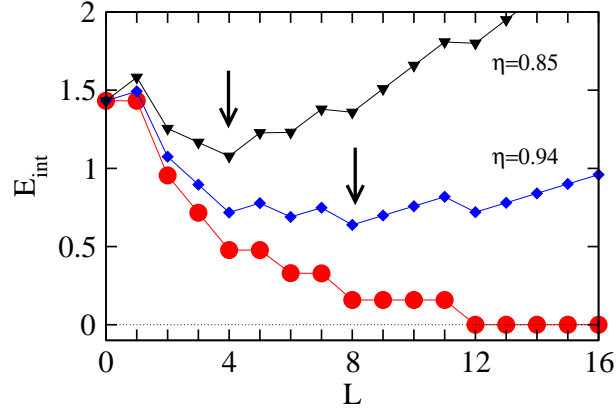


**Figure 3.** (Color online) Yrast line for  $N = 4$ , solid red circles, which corresponds to the interaction energy contribution of the lowest eigenstates for each value of  $L$ . The triangles and diamonds depict the sum of the interaction energy and the kinetic contribution for  $\eta = 0.85$  and  $\eta = 0.94$ , respectively. The arrows mark the value of  $L$  which corresponds to the GS in each case. The energies are given in units of  $\hbar\omega_{\perp}$ .

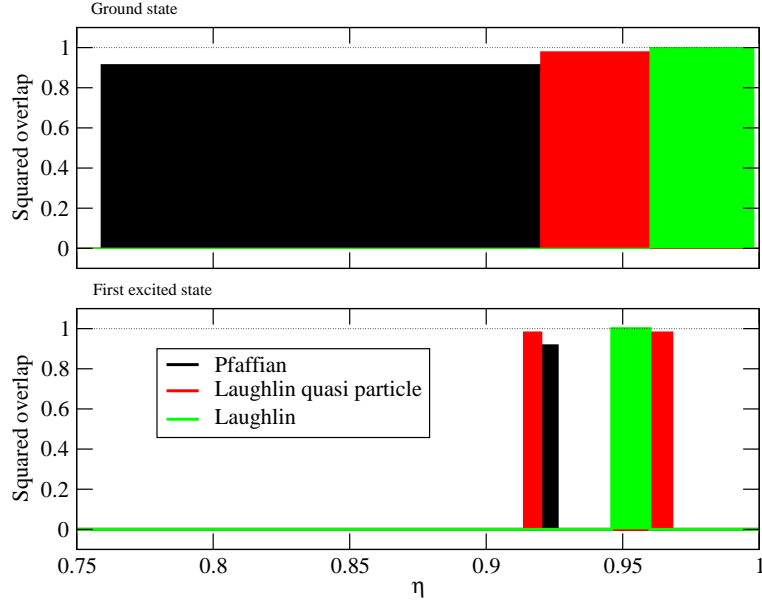


**Figure 4.** (Color online) Squared overlap between the Pfaffian, the Laughlin-quasiparticle and the Laughlin states and the ground state (upper panel) and the first excited state (lower panel). The condensed region has been omitted.  $H_{22}^{\text{eff}} = H_{22}$ .

generalized Laughlin (GL), see Eqs. (16), (21), and (23). It turns out that in all three cases the state which is proportional to  $\gamma$  is much less populated than the states proportional to  $\alpha$  and  $\beta$ . We thus neglect the contribution of this term, for simplicity. As shown in Fig. 5, overviewing all three regimes, the largest improvement by using the generalized versions occurs in the Laughlin region. Here, the total angular momentum increases continuously with  $\eta$  [21], leading to substantial occupation of the state proportional to  $\beta$ .

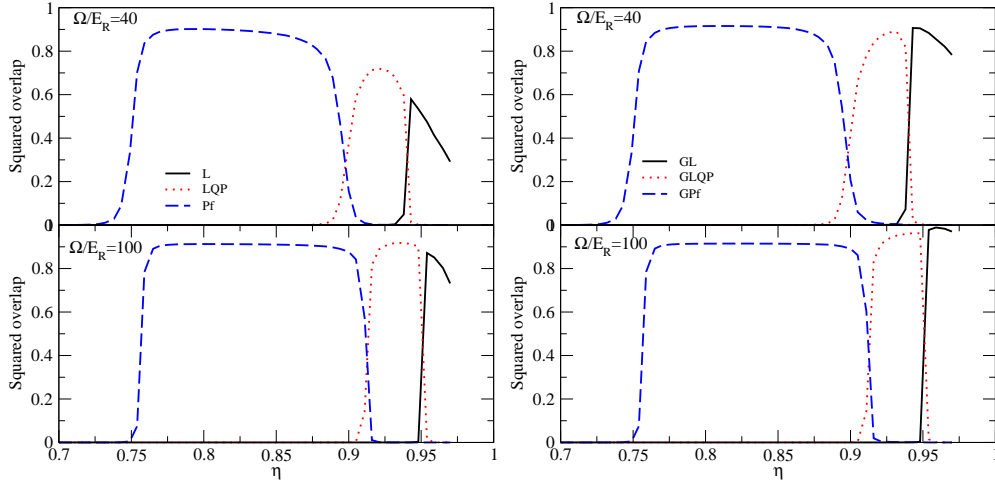


**Figure 5.** (Color online) (left panel) Squared overlap between the ground state and the original strongly correlated states considered, namely, the Pfaffian, Laughlin and Laughlin-quasiparticle states as a function of  $\eta$  for  $\hbar\Omega_0/E_R = 40$  and 100. (right panel) Squared overlap between the GS and the generalized correlated states considered, GPf, GL and GLQP as a function of  $\eta$  for  $\hbar\Omega_0/E_R = 40$  and 100.

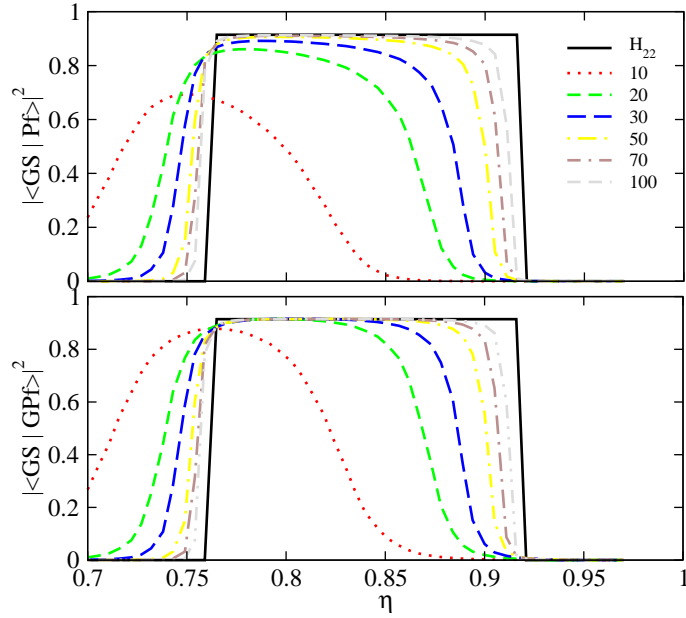


**Figure 6.** (Color online) Squared overlap between the ground state and the Pfaffian and generalized Pfaffian states defined in the text, upper and lower panels, respectively, as a function of  $\eta$ . The different lines correspond to different values of  $\hbar\Omega_0/E_R$ . The solid line is obtained with  $H_{22}^{\text{eff}} = H_{22}$ .

Detailed information about the effect of the perturbation is shown in Figs. 6, 7, and 8 for each of the three regions separately. First, in Fig. 6 we consider the overlap with the Pfaffian and GPf, exploring fairly low values of  $\hbar\Omega_0/E_R$ . Lower values of  $\hbar\Omega_0/E_R$  require the consideration of higher order terms in the expansion of  $H_{22}^{\text{eff}}$  not included in

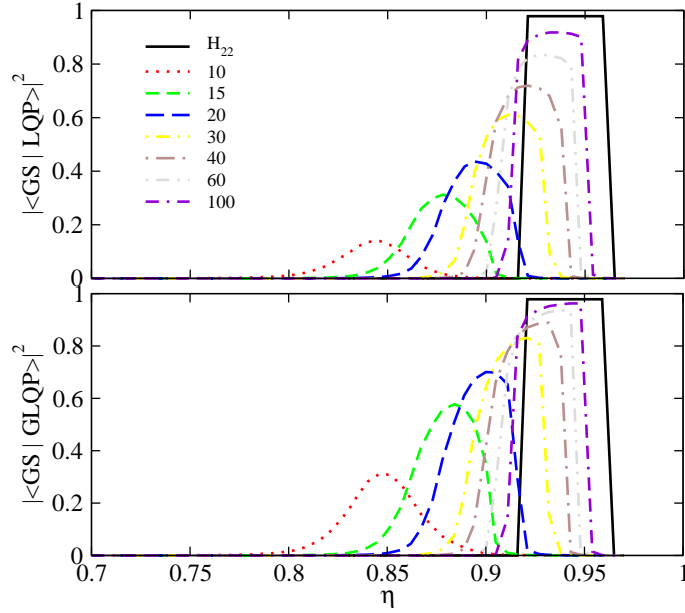


**Figure 7.** (Color online) Squared overlap between the ground state and the Laughlin-quasiparticle (LQP) and generalized Laughlin-quasiparticle (GLQP) states defined in the text, upper and lower panels, respectively, as a function of  $\eta$ . The different lines correspond to different values of  $\hbar\Omega_0/E_R$ . The solid line is obtained with  $H_{22}^{\text{eff}} = H_{22}$ .

our calculations. There one can see how by decreasing the value of  $\hbar\Omega_0$ , the  $\eta$  which provides maximum overlap becomes smaller. Thus, while in the symmetric case, the only region with non-negligible squared overlap with the Pfaffian was  $0.75 \lesssim \eta \lesssim 0.92$ , with, e.g.  $\hbar\Omega_0/E_R = 20$ , the region is roughly displaced to  $0.73 \lesssim \eta \lesssim 0.89$ .

Also, the squared overlap with the Pfaffian gets reduced, going from around 0.9 in the symmetric case, to 0.7 for  $\hbar\Omega_0/E_R = 10$ . As occurred with the Laughlin, the main effect of the perturbation is to populate states which are of the GPf type, that is, a Pfaffian core with appropriate Jastrow factors. The GPf state has a large overlap with the ground state, of the same order as the Pfaffian itself with the symmetric ground state. Interestingly, large values,  $> 0.8$ , of the squared overlap with the GPf state can be found already for  $\hbar\Omega_0/E_R > 20$ , which is relevant from the experimental point of view as it increases the window of observability.

A similar behavior is found when studying the squared overlap of the Laughlin-quasiparticle state with the exact ground state of the system. As shown in Fig. 7 the region with sizeable overlap with the Laughlin-quasiparticle state gets shifted towards lower values of  $\eta$  as we decrease  $\Omega_0$ , peaking at  $\eta = 0.85$  for  $\hbar\Omega_0/E_R = 10$ . Also, a sizeable overlap is found with the GLQP state. It is however clear, that large values of the squared overlap,  $> 0.8$ , can only be found for values of  $\hbar\Omega_0/E_R > 30$ .

In Fig. 8 we present the corresponding figure for the case of the Laughlin and generalized Laughlin states. First, we note that again the region where the L and GL are most populated gets shifted towards lower values of  $\eta$  as we decrease the

value of  $\hbar\Omega_0/E_R$ . For instance, the maximum value is obtained around  $\eta = 0.91$  for  $\hbar\Omega_0/E_R = 15$ , and this maximum is of 0.4 in the case of GL. Squared overlaps larger than 0.8 are only obtained for  $\hbar\Omega_0/E_R > 40$ . Squared overlaps larger than 0.5 can however be obtained with  $\hbar\Omega_0/E_R$  as low as 20 for  $\eta \sim 0.92$ .

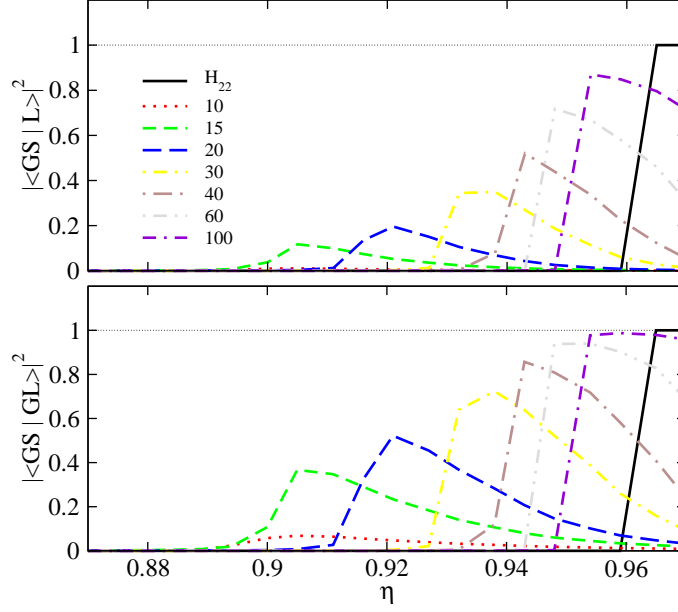


**Figure 8.** (Color online) Squared overlap between the ground state and the Laughlin (L) and generalized Laughlin (GL) states defined in the text, upper and lower panels, respectively, as a function of  $\eta$ . The different lines correspond to different values of  $\hbar\Omega_0/E_R$ . The solid line is obtained with  $H_{22}^{\text{eff}} = H_{22}$ .



## 6. Fractional charge and anyonic statistics of quasihole excitations in the Laughlin regime

An important property of the strongly correlated  $N$ -body states discussed in the previous sections are their excitations which might behave as particles with fractional charge and obey anyonic statistics, as is the case for the quasihole excitations over the Laughlin ground state [10, 15].

An experimentally feasible way of creating quasihole excitations in our system is by focusing a laser beam onto the atomic cloud. This can be described by adding the following potential to the single-particle Hamiltonian of Eq. (13) [15]:

$$\hat{V}(\xi) = I \sum_i \delta(\xi - z_i), \quad (28)$$

where  $I$  is the laser intensity, and  $\xi$  is the position onto which the beam is focused. With two such potentials we should be able to create states with two quasiholes, according to Eq. (25). In the following, we will first study quasiholes in the Laughlin state, which can be created when the system is in the adiabatic regime. Then we will also consider a slightly non-adiabatic situation, where we find quasiholes in the GL state, as defined by Eq. (26). We analyze the quasiholes in both the Laughlin and the GL state with respect to their fractional character.

### 6.1. Quasiholes' properties in the adiabatic case

As already discussed in Section 4, for  $\hbar\Omega_0 \gg E_R$ , the system's ground state squared overlap with the Laughlin state is effectively one, above the critical field strength  $\eta_2$ . Now we consider the system with the additional term (28) and find that there is also a region of  $\eta$  where the overlap of the ground state of the system and the analytical quasihole state is effectively 1, see Fig. 9. This shows that the potential of Eq. (28)

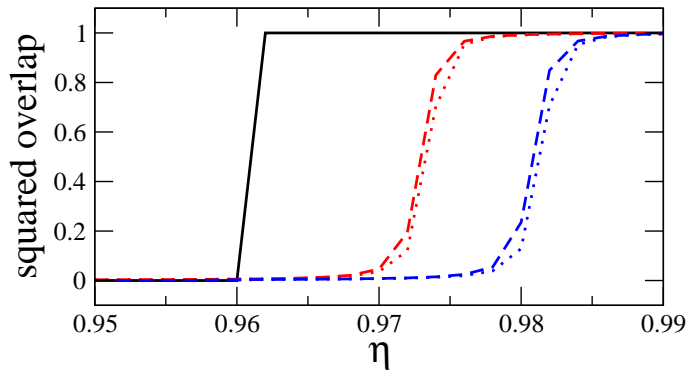


**Figure 9.** (Color online) Squared overlap of exact ground states ( $N = 4$ ) with Laughlin state (solid), Laughlin state with one quasihole (red), and Laughlin state with two quasiholes (blue). The quasiholes are created by a laser with intensity  $I = 10 \frac{\hbar\omega_{\perp}}{\lambda_{\perp}^2}$  (dotted lines) and  $I = 30 \frac{\hbar\omega_{\perp}}{\lambda_{\perp}^2}$  (dashed lines).

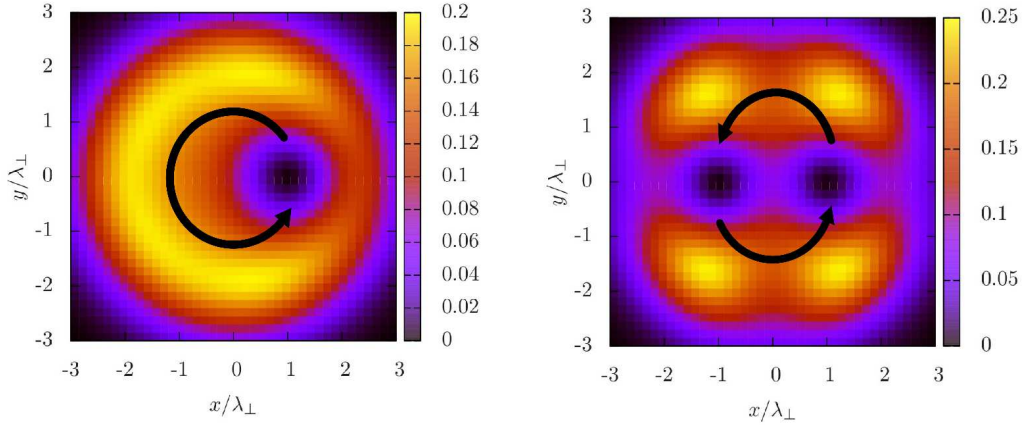


**Figure 10.** (Color online) Moving one or two quasiholes at fixed radial positions on circles around the origin allows for determining the effective charge and the statistical phase angle. The quasiholes are always fixed at a radial position  $R = 1$  (in units of  $\lambda_\perp$ ).

is able to produce quasiholes described by (24). Similarly, adding two such lasers we also find a region of  $\eta$  where the overlap between the ground state and the analytical state with two holes, Eq. (25), is very close to 1. However, we notice that the values of  $\eta$  at which the overlap for one or two quasiholes reaches 1 differ from each other, and both are found for values larger than  $\eta_2$ , see Fig. 9. These features are essentially independent of the laser strength  $I$ , for sufficiently large  $I$ .

The most interesting property of these excitations is their fractionality, i.e. fractional charge and statistics. To study the fractional charge of the quasiholes, we first note that in our electro-neutral system subjected to an artificial magnetic field, there exists the analogue of an electric charge which can be defined via the behavior of a particle or quasiparticle evolving within the gauge field. To this end, we consider the phase a quasihole picks up while being adiabatically displaced following a closed trajectory. The general expression for the Berry phase on a closed loop  $C$  is given by [38]

$$\gamma_C = i \oint_C \left\langle \Psi(\vec{R}) \left| \nabla_{\vec{R}} \right| \Psi(\vec{R}) \right\rangle \cdot d\vec{R}, \quad (29)$$

with  $|\Psi(\vec{R})\rangle$  the state of the system, characterized by a parameter  $\vec{R}$ , which in our case is the position of the quasihole. For simplicity, we now assume that the quasihole is fixed at a radial position  $|\xi| = R\lambda_\perp$ , but is moved along a circle centered at the origin, see Fig. 10, parameterized by the angle  $\phi$ . This is sufficient to test the fractional behavior.

For general contours, one can extract the acquired phases from the normalization factor of the quasihole state, as described in [39]. For our circularly symmetric contour,

however, the situation is simpler, as we can re-write Eq. (29) as

$$\gamma_C = i \int_0^{2\pi} \langle \Psi_{\mathcal{L}qh}(\phi) | \partial_\phi | \Psi_{\mathcal{L}qh}(\phi) \rangle d\phi \equiv \int_0^{2\pi} f(R) d\phi. \quad (30)$$

Here we note that, due to the circular symmetry of the Laughlin state, the integrand does not depend on the angular position of the quasihole. The function  $f(R)$  can be calculated by decomposing the Laughlin quasihole state into Fock-Darwin basis [40], which we have done analytically for particle numbers up to 6. For compactness, we explicitly give here only the result for  $N = 4$ :

$$\gamma_C = 2\pi f(R) = 2\pi \frac{4(10128R^2 + 5313R^4 + 1659R^6 + 553R^8)}{85572 + 40512R^2 + 10626R^4 + 2212R^6 + 553R^8}. \quad (31)$$

If we assume that the quasihole is moved sufficiently close to the center, i.e.  $R \lesssim 1$ , we can expand this expression in  $R$  and find,  $\gamma_C = 2\pi(0.473426R^2 + 0.0242202R^4 + \mathcal{O}(R^6)) \approx \pi R^2$ . Thus, the acquired phase is approximately given by the enclosed area in units of  $\lambda_\perp^2$ .

To obtain the effective charge of the quasihole, we must compare this result with the geometric phase acquired by a particle moved along the same closed contour due to the gauge field. In the Laughlin regime, where  $\eta \approx 1$ , we find with Eq. (14)  $B_0 \approx 2\frac{\hbar}{\lambda_\perp}$ , thus the acquired phase  $\varphi$  is two times the enclosed area in units of  $\lambda_\perp^2$ , i.e.  $\varphi = \frac{1}{\hbar} B_0 (R\lambda_\perp)^2 \pi \approx 2R^2 \pi$ . From this follows the effective charge of the quasihole to be  $q_{\text{eff}} = \frac{\gamma_C}{\varphi} \sim 0.47$ , close to the expected value for the Laughlin state at half filling in the thermodynamic limit,  $1/2$  [7, 10]. We have performed a similar study for  $N = 5$  and  $N = 6$ , finding that for  $N = 5$ , the effective charge is about 0.48, and for  $N = 6$  it is found to be 0.49, i.e. by increasing the particle number the value  $1/2$  is approached.

### 6.1.1. Fractional statistics

To prove the fractional statistics of the quasihole excitations we now consider the system with two quasiholes at  $\xi_1 = |\xi_1|e^{i\phi_1}$  and  $\xi_2 = |\xi_2|e^{i\phi_2}$ , which we assume to sit on opposite radial positions, i.e.  $|\xi_1| = |\xi_2| = R\lambda_\perp$  and  $\phi_2 - \phi_1 = \pi$ . We now consider the simultaneous adiabatic movement of the two quasiholes on two half circles, in such a way that, at the end, the quasiholes interchange position (see Fig. 10). This differs from a more common setup to test the statistical angle, where one quasihole is fixed in the center, while the other is encircling it, but it has the advantage that it maximizes the distance between the two quasiholes. Note that in Fig. 10, the radial position is chosen at  $R = 1$ , i.e. the distance between the center of the quasiholes is  $2\lambda_\perp$ , which seems to be the minimum distance needed for not having a significant overlap ( $< 10\%$ ) between the two quasiholes, see Fig. 11(a). On the other hand, in this small system of just four particles, larger radial positions lead to quasiholes overlapping with the systems edge.

The total phase picked up during the described movement should be the sum of the phase picked up by one quasihole moved along a circle plus a phase factor due to the interchange of the two quasiholes. Again the phase gradient turns out to be

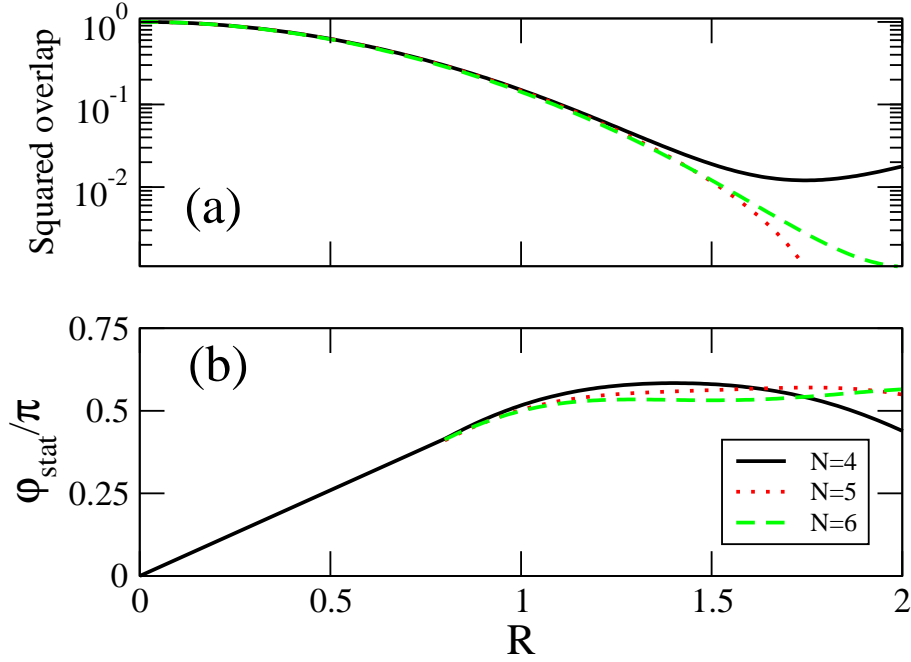


**Figure 11.** (Color online) (a) Squared overlap between the quasihole wave functions,  $|\langle \Psi_{\mathcal{L}qh}(\xi_1) | \Psi_{\mathcal{L}qh}(\xi_2) \rangle|^2$  at opposite angular positions,  $\phi_1 - \phi_2 = \pi$ , as a function their distance to the center,  $|\xi_1| = |\xi_2| = R\lambda_{\perp}$ . (b) Statistical angle of two quasiholes at opposite angular positions and radial position  $R\lambda_{\perp}$ . In both panels we present results for  $N = 4$  (black solid),  $N = 5$  (red dotted), and  $N = 6$  (green dashed).

independent from the angular position, but is described by a different function  $\tilde{f}$  of the radial coordinate:

$$\tilde{f}(R) = \frac{8(2868120R^4 + 461616R^8 + 25242R^{12} + 553R^{16})}{41660640 + 11472480R^4 + 923232R^8 + 33656R^{12} + 553R^{16}}. \quad (32)$$

The statistical phase angle is thus,

$$\varphi(R)_{\text{stat}} \equiv \int_0^{2\pi} f(R) d\phi - \int_0^{\pi} \tilde{f}(R) d\phi = 2\pi f(R) - \pi \tilde{f}(R). \quad (33)$$

It is shown, as a function of  $R$ , in Fig. 11 (b). First, as expected the statistical phase is zero if both quasiholes are in the same position, and it increases linearly as the distance between the quasiholes is increased. This linear behavior then saturates once the overlap between the two quasiholes,  $|\langle \Psi_{\mathcal{L}qh}(\xi_1) | \Psi_{\mathcal{L}qh}(\xi_2) \rangle|^2$ , drops below 0.1, and remains mostly constant around  $\pi/2$ . By increasing the number of particles  $N$ , the phase angle become less dependent on  $R$  once the two quasiholes do not overlap, meaning that it becomes a robust property of the quasiholes. It stabilizes around the expected value of  $\pi/2$ . At larger distances  $R$ , the system's edge starts to play a role.

## 6.2. Non-adiabatic effects on the properties of quasiholes

To study the fractionality of quasihole excitations in the non-adiabatic case we will again profit from the generalized analytical representations used to describe the ground state

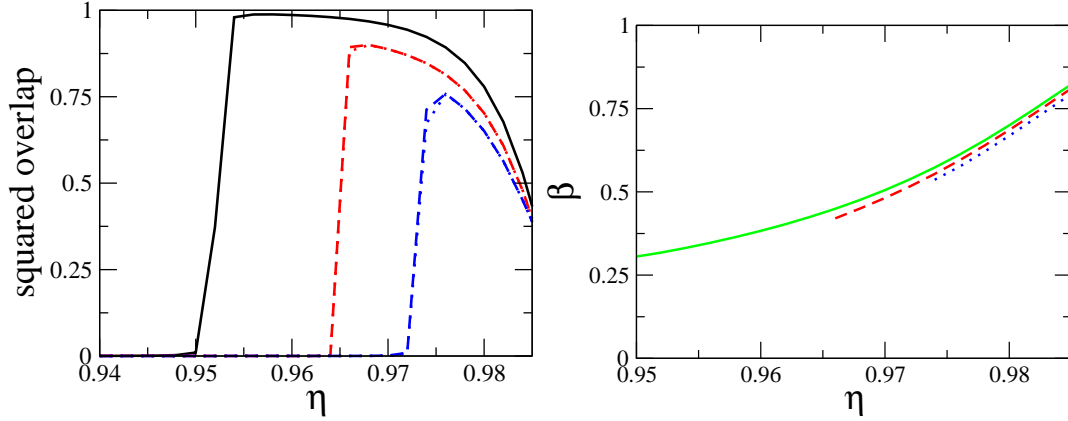


**Figure 12.** (Color online) Left: Squared overlap of exact ground states ( $N = 4$ ) with generalized Laughlin state (solid black), generalized Laughlin state with one quasihole (red), and generalized Laughlin state with two quasiholes (blue). The quasiholes are created by a laser with an intensity  $I = 30 \frac{\hbar\omega_{\perp}}{\lambda_{\perp}^2}$  (dotted lines) and  $I = 50 \frac{\hbar\omega_{\perp}}{\lambda_{\perp}^2}$  (dashed lines) at  $\xi_1 = \lambda_{\perp}$  and  $\xi_2 = -\lambda_{\perp}$ . The Rabi frequency is  $\hbar\Omega_0 = 100E_R$ . Right: The values of the variational parameter  $\beta$  for a given  $\eta$  are similar for all three states.

of the system. Following the discussion in the previous section we compute the squared overlap of the ground state obtained with no-, one-, and two-extra lasers piercing holes into the system. First, we find a significant squared overlap for the slightly perturbed case at  $\hbar\Omega_0 = 100E_R$ , see Fig. 12. As occurred in the adiabatic case, a large overlap with the analytical one- and two-quasihole states appears only at higher field strengths than the one at which the generalized Laughlin state is reached. Our study of the properties of quasiholes in the non-adiabatic case will be restricted to the parameter domain where a fair description of the states is provided by the generalized state given in Sec. 3.

We now test the behavior of the quasiholes in a generalized Laughlin state. This can be done as before, but now we must note that the gradient of the state will not only depend on the radial, but also on the angular position of the quasiholes. Furthermore, it will depend on the parameter  $\beta$  as defined in Eqs. (26) and (27), which is used to improve the overlap. As shown in Fig. 12, for given parameters  $\eta$  and  $\Omega_0$  the same value for  $\beta$  optimizes simultaneously the ground state, the quasihole state, and the state with two quasiholes. We define

$$f_{\beta}(R, \phi) \equiv \langle \Psi_{\mathcal{L}q\hbar}(\phi) | \partial_{\phi} | \Psi_{\mathcal{L}q\hbar}(\phi) \rangle. \quad (34)$$

This function  $f_{\beta}$  is quite lengthy, so we expand it in  $R$  and give only the lowest term ( $\mathcal{O}(R^2)$ ):

$$f_{\beta}(R, \phi) \simeq \frac{8115904 + 2799526\beta^2 - 7102\sqrt{94958(1-\beta^2)}\beta \cos(2\phi)}{17142924 + 4477401\beta^2} R^2 \quad (35)$$

From the expression we see that for a fixed and small value of  $R$ ,  $f_{\beta}$  oscillates around  $R^2/2$ , such that the angular integration  $\int_0^{2\pi} f_{\beta}(R, \phi) d\phi$  again will yield a Berry phase close to the encircled area, thus half of the Berry phase accumulated by a normal particle.

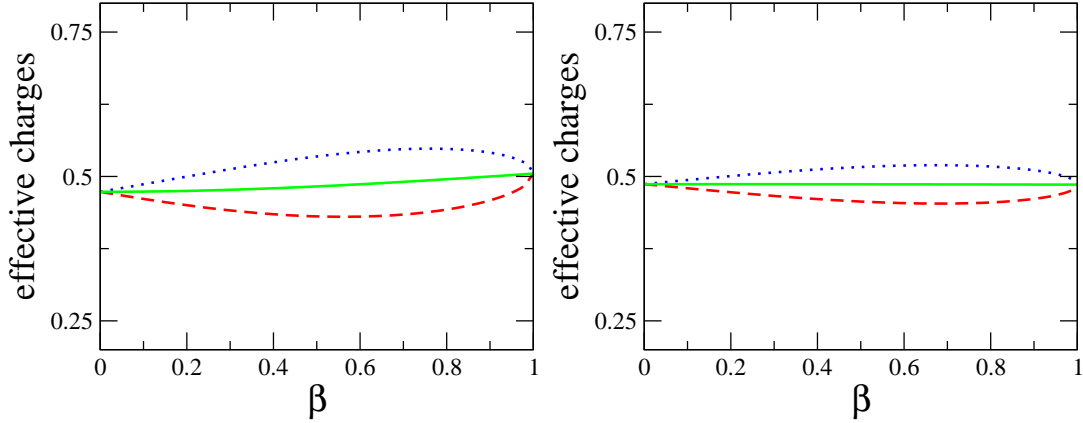


**Figure 13.** The effective charges  $q_y$  (blue dotted) and  $q_x$  (red dashed), and  $q_{\text{eff}} = (q_x + q_y)/2$  (green solid) of quasiholes in the generalized Laughlin state as a function of the admixture  $\beta$  of higher angular momentum to the Laughlin state, for  $N = 4$  (left) and  $N = 6$  (right).

Formally, we can capture this oscillating behavior by defining two effective charges  $q_x$  and  $q_y$ , depending on the direction in which the quasihole moves. With this and by generalizing to arbitrary loops the Berry phase in the limit of small radial positions  $R \lesssim 1$ , the Berry phase can be written as,

$$\gamma_C = \oint \frac{1}{\lambda_{\perp}^2} (q_x y, -q_y x) \cdot d\vec{r} = (q_x + q_y) \frac{A}{\lambda_{\perp}^2}, \quad (36)$$

where  $A$  is the encircled area and Stokes' theorem has been applied. An effective charge can be defined simply as,  $q_{\text{eff}} = (q_x + q_y)/2$ . The values of  $q_x$ ,  $q_y$ , and  $q_{\text{eff}}$  are plotted as a function of  $\beta$  in Fig. 13 for different  $N$ . As can be seen, in all cases the effective charges are close to  $1/2$ . For small values of  $\beta$ , which represent realistic states of the system, the value of the charges gets closer to  $1/2$  as the number of atoms in the system is increased. In summary, the average charge  $q_{\text{eff}}$  has only a minor dependence on  $\beta$ , which decreases as  $N$  increases. Though not realized in our system, we note that in the limit  $\beta \rightarrow 1$ , both charges  $q_x$  and  $q_y$  again coincide due to the recovered cylindrical symmetry of the state  $\Psi_{\mathcal{L}1}$ .

Finally we introduce two quasiholes into the generalized Laughlin state. Following a procedure similar to the one for the adiabatic case presented in the previous section, we extract the statistical phase angle of the quasiholes. The result as a function of  $\beta$  is shown in Fig. 14 for  $N = 4$  and closed paths of different radii. While the quasiholes in the bulk,  $R = 1$ , remain with an almost constant phase angle  $\varphi_{\text{stat}} \approx 0.51$ , the phase angle of quasiholes closer at the edge of the system have a stronger dependence on  $\beta$ . Thus, we find that the presence of a certain degree of non-adiabaticity,  $\beta \leq 0.7$  does not spoil the presence of anyonic quasihole excitations of the Laughlin state.

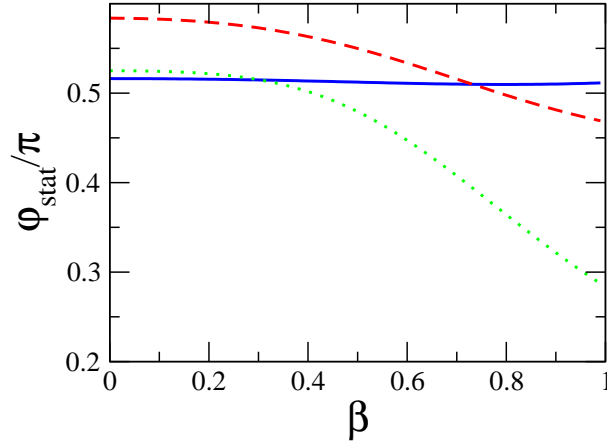


**Figure 14.** (Color online) Statistical phase angle  $\varphi_{\text{stat}}$  for two quasiholes in generalized Laughlin state as a function of the variational parameter  $\beta$ . The radial position of the quasiholes is at  $\lambda_{\perp}$  (blue solid line),  $1.4\lambda_{\perp}$  (red dashed line), and  $1.8\lambda_{\perp}$  (green dotted line).

## 7. Evolution with $N$ of the energy gap

The typical scenario of an experiment that has as a goal the realization of a specific strongly correlated state, is to first prepare an easily attainable initial state. Then, one may follow adiabatically a route in parameter space which ends up in the final desired state [16, 20]. This final state is expected to be robust, with a mean-life time larger than the time necessary to perform the measurements. A crucial ingredient necessary for the success of such approach is to have energy gaps as large as possible over all the ground states involved along the route.

In this section we concentrate on the study of the energy gap over the Laughlin state. We consider first the adiabatic case and then study the effect of the perturbation on the energy gap. The gap is the energy difference between the ground state and the lowest excitation in the thermodynamic limit. We take the thermodynamic limit by increasing  $N$  keeping the chemical potential constant during the process. In the homogeneous  $2D$  case this corresponds to fixing  $gN = \text{constant}$ , our calculations are performed fulfilling this relation. We will analyze the behavior of the gap for increasing  $N$  by means of our exact diagonalization calculations up to  $N = 7$ .

For the Laughlin state in the adiabatic/symmetric case, as is shown in Fig. 2 for  $N = 4$  and  $L = 12$  there are two lowest excitations with  $L = 12 - 4 = 8$  and  $L = 13$  depending on the value of  $\eta$ . This is a general result for any  $N$ , the excitations have  $L = N(N - 1) - N$  and  $L = N(N - 1) + 1$ . The excitation with  $L = 13$  is an excitation of the center of mass of the system. This is due to the incompressibility of the Laughlin state. Namely, as shown in Fig. 3, the state can increase its angular momentum without changing its interaction energy. We ignore this excitation, since we are interested in bulk excitations. This means that the linear left branch in the Laughlin region in Fig. 2 must be extended up to  $\eta = 1$  (where one has the largest gap). All the branches on the right



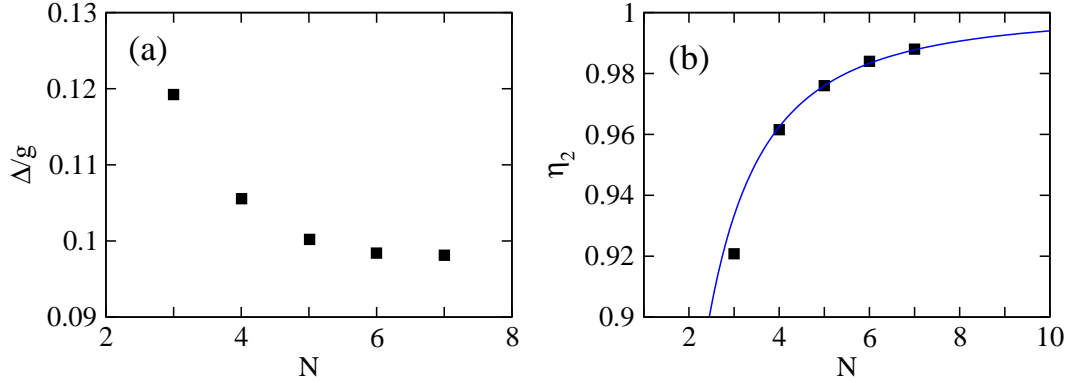


**Figure 15.** (Color online) (a)  $\Delta/g$ , in units of  $\hbar\omega_\perp$ , of the Laughlin state as a function of  $N$  in the adiabatic/symmetric case. (b) Value of  $\eta_2$  computed for  $N = 3, 4, 5, 6$ , and  $7$  in the adiabatic/symmetric case, compared to the prediction explained in the text,  $\eta_2 = 1 - 0.1(gN/N^2)$ .

that would lie below this line, are edge excitations of different polarity. In addition, the energy of the first excited state over the Laughlin denoted as  $\Delta$ , with  $L = N(N - 1)$  (i.e., in the same  $L$ -subspace) coincides with this largest gap at  $\eta = 1$  where effectively there is no trap.

As a consequence, to see the evolution of the gap over the Laughlin state it is sufficient to calculate the first two eigenvalues of the energy spectrum in the  $L = N(N - 1)$  subspace for each  $N$ . In Fig. 15(a) we show the evolution of  $\Delta/g$  with  $N$ . The tendency up to  $N = 7$  is to asymptotically recover the value of 0.1 previously obtained by Regnault *et al.* [36] assuming a toroidal geometry and later reproduced by Roncaglia *et al.* [19]. Since we have taken  $gN = 6$ , then  $\Delta$  must compensate this  $N$ -dependence and consequently tend to zero as  $\Delta \sim 1/N$ . In effect, our results imply that the bosonic Laughlin state is observable only for few number of particles.

For possible practical implementations, it is also important to quantify the size of the parameter region where the Laughlin can be produced. Therefore, a good estimate of  $\eta_2$  can be obtained taking advantage of the abovementioned coincidence.  $\eta_2$  is the critical value where the energies of the Laughlin and  $L = N(N - 1) - N$  state cross, or

$$(1 - \eta_2)(L_0 - N)\hbar\omega_\perp + V_1 = (1 - \eta_2)L_0\hbar\omega_\perp + V_0 \quad (37)$$

where  $L_0 = N(N - 1)$  and  $V_0$  and  $V_1$  are  $E_{\text{int}}(L_0)$  and  $E_{\text{int}}(L_0 - N)$  (see Fig. 3), respectively. Or,

$$\eta_2 = 1 - \frac{V_1}{N\hbar\omega_\perp} \quad (V_0 = 0). \quad (38)$$

In addition,  $V_1$  coincides with the energy difference  $\Delta$  between the ground state and the first excitation in the  $L_0$  subspace which tends, as  $N$  increases (see Fig. 15)(a), to

$$\Delta \sim 0.1g\hbar\omega_\perp = 0.1(6/N)\hbar\omega_\perp \quad (39)$$

and then

$$\eta_2 = 1 - \Delta/(N\hbar\omega_\perp) \sim 1 - 0.1\frac{gN}{N^2}. \quad (40)$$

In Fig. 15(b) we compare the prediction of this formula and the computed  $\eta_2$  for different  $N$ . As can be seen the formula agrees very well with the numerically obtained values.

Finally, Fig. 16 shows the change of the gap with decreasing  $\Omega_0$ . There are some important differences between the symmetric and the perturbed cases. The perturbation mixes a large number of subspaces and now it is not possible to ignore the right branch. The initial ( $\eta_2$ ) and final frequencies at the boundaries of the Laughlin region are shifted to smaller values. The largest gap, the one at the upper vertex of the triangle is nearly constant. At  $\eta_2$  the perturbation opens a gap where degeneracy occurs in the symmetric case. As a consequence, we conclude that on the one hand, the perturbation favors the observability, and on the other hand, the detection has to be restricted to a small number of particles.

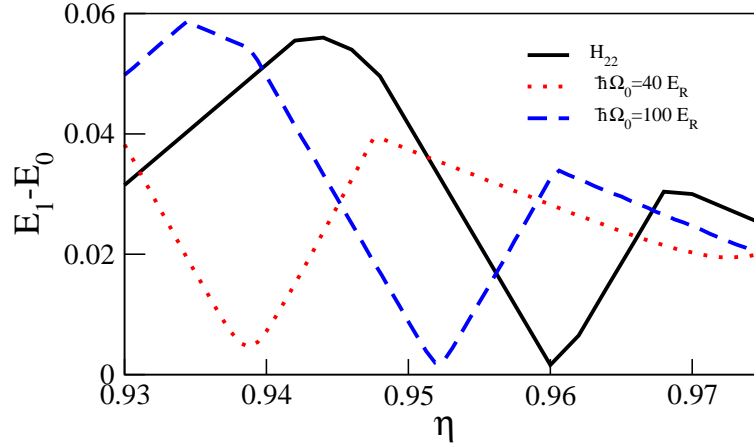


**Figure 16.** (Color online) Evolution of the energy gap, in units of  $\hbar\omega_{\perp}$  with decreasing  $\Omega_0$  in the Laughlin region.

## 8. Summary and conclusions

We have studied the possibility of producing relevant strongly correlated quantum states as ground states of a system of ultracold two-level atoms subjected to an artificial gauge field. The focus is on the formation of Moore-Read (Pfaffian), Laughlin and Laughlin-quasiparticle states. Considering a few number of atoms we have shown by exact diagonalization methods, that large squared overlaps between Pfaffian-like, Laughlin-quasiparticle-like and Laughlin-like states and the ground state of the system are found even for fairly small values of the external laser intensity  $\hbar\Omega_0/E_R$ . Reducing the laser intensity, correspondingly reducing the Rabi frequency, induces deformation in the system, increasing the angular momentum of the states. The structure of these deformed states is such that the main properties of the original undeformed states is retained in a broad region of parameter space. An analytical representation of the ground states consisting on the original states supplemented by a term affected by Jastrow factors increasing in two units their angular momentum provides large overlap

with the numerical results, and allows to get analytical insights into the fractional behavior of the quasihole excitations.

We have checked that quasihole states on the Laughlin and generalized Laughlin states can be produced by means of additional laser beams. We have studied the fractional charge and anyonic statistics of such quasiholes making use of the analytical representation of the states. Both, the effective charge and the statistical phase angle are close to the expected value of  $1/2$ , even for the small number of particles considered here. Such fractional behavior is found whenever quasiholes are able to evolve in the bulk of the system, thus, the agreement with the expected behavior gets better as the size of the system is increased. The admixture of higher angular momentum in the generalized Laughlin state does not modify the fractional behavior of its quasihole excitation. However, as the creation of two quasiholes requires a higher artificial field strength  $\eta$  than the one necessary to get into the (generalized) Laughlin regime, our analysis is relevant mostly in the weakly perturbed regime, whereas in the highly perturbed regime an exact numerical evolution of the adiabatic movement would be needed, falling beyond the scope of the present work.

Concerning the observability of Laughlin-like states, we find that decreasing  $\hbar\Omega_0/E_R$  shifts the spectrum to smaller values of  $\eta$ , which are thus further away from the instability region  $\eta = 1$ , favoring the experimental conditions. In addition, keeping the chemical potential constant, i.e.  $Ng = \text{constant}$ , we find that the observability of the Laughlin state is reduced to small number of particles due to the fast decrease of the largest possible gap over the ground state as  $N$  increases.

An interesting aspect for future investigation are the excitations in the Pfaffian-like regime, which might obey non-Abelian statistics. A signature for this behavior would be a degeneracy in the state with four quasiholes [41]. However, our present system is too small to test this physics.

## Acknowledgments

The authors thank N. Cooper, J. Dalibard and K. J. Günter for useful comments and discussions. This work has been supported by EU (NAMEQUAM, AQUTE, MIDAS), ERC (QUAGATUA), Spanish MINCIN (FIS2008-00784, FIS2010-16185, FIS2008-01661 and QOIT Consolider-Ingenio 2010), Alexander von Humboldt Stiftung, IFRAF and ANR (BOFL project). B. J.-D. is supported by a Grup Consolidat SGR 21-2009-2013. M. L. acknowledges Hamburg Theory Award.

## Appendix A. Effective Hamiltonian

Let us consider a system described by a single particle Hamiltonian given by  $H = H_0 + V$  where  $H_0$  is solvable and  $V$  can be treated as a perturbation. In addition, let us assume that the eigenvalues of  $H_0$  are grouped in manifolds well-separated in energy, i.e., the eigenenergies  $E_{i\alpha}$  have the following property,

$$|E_{i\alpha} - E_{j\alpha}| \ll |E_{i\alpha} - E_{j\beta}| \quad (\text{A.1})$$

where  $\alpha$  and  $\beta$  denote different manifolds and the index  $i$  denotes different states inside a manifold. In our case we have two manifolds, the lowest energy one ( $\alpha = 2$ ) described by  $H_{22}$  and the most energetic one described by  $H_{11}$  ( $\beta = 1$ ), both together play the role of  $H_0$ ,

$$H_0 = \begin{pmatrix} H_{11} & 0 \\ 0 & H_{22} \end{pmatrix} \quad (\text{A.2})$$

acting on the spinor shown below Eq.( 6).

The difference in energy,  $\hbar\Omega_0$ , is much larger than the typical expected values of  $H_{22}$  which are of the order of the recoil energy  $E_R = \hbar^2 k^2 / 2M$ . Within the lowest manifold we make the LLL assumption. This scenario is valid in the case where the two internal states are uncoupled and the system evolves always in  $|\psi_1\rangle$  or  $|\psi_2\rangle$ .

Instead, if there is coupling between the manifolds, the Hamiltonian is represented by  $H_0 + \lambda V$  where  $\lambda$  is a dimensionless parameter and  $V$ , in general, has non-zero matrix elements inside each manifold as well as between them. As long as  $\lambda$  is small, the structure of the well-separated manifolds and their degeneracy is preserved with slight modifications. Physically, the coupling between the two manifolds means that the motion of an atom in  $|\psi_2\rangle$  is slightly modified by a sudden and short time period in the other manifold. The high frequency dynamics driven by  $(E_{i\alpha} - E_{i\beta})/\hbar$  ( $\alpha \neq \beta$ ) is averaged by the slow dynamics driven by  $(E_{i\alpha} - E_{j\alpha})/\hbar$ . In a way, the wave functions of the manifold-2 are “influenced” (or dressed) by the wave functions of manifold-1. In our case, the structure of  $V$  is,

$$V = \begin{pmatrix} 0 & H_{12} \\ H_{21} & 0 \end{pmatrix}, \quad (\text{A.3})$$

with no diagonal elements.

The main goal will be to obtain an effective Hermitian Hamiltonian  $H'$  that acts only on the unperturbed manifold-2, though having the same eigenvalues as those of  $H$ , and with zero matrix elements between the two unperturbed manifolds. In this way, we will be able to consider only the FD functions and ignore manifold-1.

The Hermiticity and the coincidence on the eigenvalues with  $H$  are achieved if we consider a unitary transformation from  $H$  to  $H'$  as,

$$H' = T H T^\dagger \quad (\text{A.4})$$

where  $T = e^{iS}$  and  $S = S^\dagger$ . Or

$$\begin{aligned} H' &= e^{iS} H e^{-iS} \\ &= H + [iS, H] + \frac{1}{2!} [iS, [iS, H]] + \dots = H_0 + \lambda H'_1 + \lambda^2 H'_2 + \dots \end{aligned} \quad (\text{A.5})$$

where we have considered the expansion  $S = \lambda S_1 + \lambda^2 S_2 + \dots$  and the condition that  $S$  has zero matrix elements inside each manifold. Grouping the terms in orders of  $\lambda$ , it is possible to solve  $S_i$  step by step as functions of known quantities. One arrives to the expression:

$$\begin{aligned} \langle i\alpha | H' | j\alpha \rangle &= E_{i\alpha} \delta_{ij} + \langle i\alpha | \lambda V | j\alpha \rangle + \frac{1}{2} \sum_{k, \gamma \neq \alpha} \langle i\alpha | \lambda V | k\gamma \rangle \langle k\gamma | \lambda V | j\alpha \rangle \\ &\times \left[ \frac{1}{E_{i\alpha} - E_{k\gamma}} + \frac{1}{E_{j\alpha} - E_{k\gamma}} \right] + \dots \end{aligned} \quad (\text{A.6})$$

The first term represents the unperturbed levels in the manifold-2, the second one is the direct coupling between unperturbed levels in the manifold-2 and the third term is the contribution of the indirect coupling through the manifold-1. In our case the last equation reduces to,

$$\langle i\alpha | H' | j\alpha \rangle \simeq E_{i2} \delta_{ij} + \frac{\lambda^2}{2} \sum_k \langle i2 | V | k1 \rangle \langle k1 | V | j2 \rangle \left( -\frac{1}{\Omega_0} - \frac{1}{\Omega_0} \right) \quad (\text{A.7})$$

where we have approximated  $E_{k1}$  by  $\hbar\Omega_0$  and considered  $E_{i2} \ll \hbar\Omega_0$  or

$$\langle i\alpha | H' | j\alpha \rangle = E_{i2} \delta_{ij} - \frac{\lambda^2}{\Omega_0} \langle i2 | V^2 | j2 \rangle \quad (\text{A.8})$$

thus,

$$H' = H_{22} - \frac{H_{21}H_{12}}{\Omega_0} \quad (\text{A.9})$$

which is the results used in Eq. (12) in Section 2. The interaction term is considered part of the non-perturbed term together with the kinetic contribution, see Eq. (13).

The explicit form of the perturbation term  $H_{21}H_{12}$  used is,

$$\begin{aligned} H_{21}H_{12} &= \left( \frac{\hbar^4}{4M^2w^4} - \frac{2x^2\hbar^4}{M^2w^6} + \frac{k^2x^2\hbar^4}{16M^2w^4} + \frac{k^4x^2\hbar^4}{64M^2w^2} \right. \\ &\quad \left. + \frac{ikxy\hbar^4}{4M^2w^5} + \frac{k^2y^2\hbar^4}{64M^2w^4} \right) \\ &\quad + \left( -\frac{ikx\hbar^4}{4M^2w^3} - \frac{ik^3x\hbar^4}{8M^2w} \right) \partial_y + \left( \frac{x\hbar^4}{M^2w^4} - \frac{iky\hbar^4}{8M^2w^3} \right) \partial_x \\ &\quad + \left( -\frac{k^2\hbar^4}{4M^2} + \frac{k^2x^2\hbar^4}{4M^2w^2} \right) \partial_y^2 + \left( -\frac{\hbar^4}{4M^2w^2} + \frac{x^2\hbar^4}{2M^2w^4} \right) \partial_x^2. \end{aligned} \quad (\text{A.10})$$

one can show that this operator does not conserve  $L$ , as it connects  $L'$ -subspaces with  $L' = L + \Delta$  where  $\Delta = 0, \pm 2, \pm 4$ .

## References

- [1] M.H. Anderson, J.R. Ensher, M.R. Matthews, C.E. Wieman, and E.A. Cornell, *Science*, **269**, 198 (1995).
- [2] K.B. Davis, M.-O. Mewes, M.R. , N.J. van Druten, D.S. Durfee, D.M. Kurn, and W.Ketterle, *Phys. Rev. Lett.* **75**, 3969 (1995).
- [3] M.R. Andrews, C.G. Townsend, H.-J. Meisner, D.S. Durfee, D.M. Kurn, and W. Ketterle, *Science* **275**, 637 (1997).
- [4] M. Lewenstein, A. Sanpera, V. Ahufinger, B. Damski, A. Sen (De) and U. Sen, *Adv. Phys.* **56**, 243 (2007).
- [5] M. Greiner, O. Mandel, T. Esslinger, T. W. Hänsch, and I. Bloch, *Nature* **415**, 39 (2002).
- [6] G. Moore and N. Read, *Nucl. Phys.* **B360**, 362 (1991).
- [7] R.B. Laughlin, *Phys. Rev. Lett.* **50**, 1395 (1983).
- [8] N.K. Wilkin and J.M.F. Gunn, *Phys. Rev. Lett.* **84**, 6 (2000).
- [9] N.R. Cooper, and N.K. Wilkin, *Phys. Rev. B* **60**, R16279 (1999).
- [10] D.J. Arovas, J.R. Schrieffer, and F. Wilczek, *Phys. Rev. Lett.* **53**, 722 (1984).
- [11] C. Nayak and F. Wilczek, *Nucl. Phys. B* **479**, 529 (1996).
- [12] E.H. Rezayi and N. Read, *Phys. Rev. B* **56**, 16846 (1996).
- [13] C. Nayak, S. H. Simon, A. Stern, M. Freedman, and S. Das Sarma, *Rev. Mod. Phys.* **80**, 1083 (2008).
- [14] K.W. Madison, F. Chevy, V. Bretin, and J.Dalibard, *Phys. Rev. Lett.* **86**, 4443 (2001).
- [15] B. Paredes, P. Fedichev, J.I. Cirac, and P. Zoller, *Phys. Rev. Lett.* **87**, 010402 (2001).
- [16] M. Popp, B. Paredes and J.I.Cirac, *Phys.Rev.* **A70**, 053612 (2004).
- [17] I. Bloch, J. Dalibard and W. Zwerger, *Rev. Mod. Phys.* **80**, 885 (2008).
- [18] K. J. Günter, M. Cheneau, T. Yefsah, S. P. Rath, and J. Dalibard, *Phys. Rev. A* **79**, 011604(R) (2009).
- [19] M. Roncaglia, M. Rizzi, J. Dalibard, *Sci. Rep.* **1**, 43 (2011).
- [20] M. Roncaglia, M. Rizzi and J.I. Cirac, *Phys. Rev. Lett.* **104**, 096803 (2010).
- [21] B. Juliá-Díaz, D. Dagnino, K.J. Günter, T. Graß, N. Barberán, M. Lewenstein, and J.Dalibard, in print *Phys. Rev. A*, cond-mat/1105.5021.
- [22] Frank Wilczek and A. Zee, *Phys. Rev. Lett.* **52**, 2111 (1984).
- [23] G. Juzeliunas and P. Öhberg, *Phys. Rev. Lett.* **93**, 033602 (2004).
- [24] J. Ruseckas, G. Juzeliunas, P. Öhberg, and M. Fleischhauer, *Phys. Rev. Lett.* **95**, 010404 (2005).
- [25] T. Kinoshita, T. Wenger, and D.S. Weiss, *Nature* **440**, 900 (2006).
- [26] N. Gemelke, E. Sarajlic, S. Chu, arXiv:1007.2677 (2010).
- [27] C. Cohen-Tannoudji, J. Dupont-Roc, and G. Grynberg, *Atom-Photon Interactions* (Wiley, New York, 1992).
- [28] J.L. Basdevant, and J. Dalibard, *The Quantum Mechanics Solver* (Springer, The Netherlands, 2006).
- [29] J. Dalibard, F. Gerbier, G. Juzeliūnas, and P. Öhberg, in print *Reviews of Modern Physics*, arXiv:1008.5378.
- [30] M.I. Parke, N.K.Wilkin, J.M.F. Gunn, and A. Bourne, *Phys. Rev. Lett.* **101**, 110401 (2008).
- [31] D. Dagnino, N. Barberán, M. Lewenstein, and J. Dalibard, *Nature Phys.* **5**, 431 (2009).
- [32] L. Jacak, P. Hawrylak, and A. Wojs, *Quantum Dots* (Springer, Berlin, 1998).
- [33] N.R. Cooper, *Adv. Phys.* **57**, 539 (2008).
- [34] A.L. Fetter, *Rev. Mod. Phys.* **81**, 647 (2009).
- [35] N. R. Cooper, N. K. Wilkin, and, J. M. F. Gunn, *Phys. Rev. Lett.* **87** 120405 (2001).
- [36] N. Regnault and T. Jolicoeur, *Phys. Rev. Lett.* **91** 030402 (2003).
- [37] M. A. Cazalilla, *Phys. Rev. A* **67**, 063613 (2003).
- [38] M. V. Berry, *Proc. R. Soc. Lond. A* **392**, 45 (1984).
- [39] X.-G. Wen, *Quantum Field Theory of Many-Body Systems*, Oxford University Press (2004).

[40] B. Juliá-Díaz, and T. Graß, in preparation (2011).

[41] E. Fradkin, C. Nayak, A. Tsvelik, and F. Wilczek, Nucl. Phys. B **516**, 704 (1998).